crystals

MDPI

Article

Optical Properties and Band Gap of Ternary PSN-PMN-PT Single Crystals

Wei Long [1], Xing Fan [1,2], Pinyang Fang [1], Xiaojuan Li [1,*] and Zengzhe Xi [1,*]

[1] Shaanxi Key Laboratory of Photoelectric Functional Materials and Devices, School of Materials and Chemical Engineering, Xi'an Technological University, Xi'an 710021, China; longwei@xatu.edu.cn (W.L.); fanxingabcd@163.com (X.F.); fpy_2000@163.com (P.F.)

[2] National Laboratory of Solid State Microstructures, Department of Materials Science and Engineering, College of Engineering and Applied Sciences, Nanjing University, Nanjing 210093, China

* Correspondence: lixiaojuan28@163.com (X.L.); zzhxi@xatu.edu.cn (Z.X.)

Abstract: This study investigated the optical properties and the interband transition of a ternary [100]-oriented 6PSN-61PMN-33PT relaxor ferroelectric single crystal. Compared with the binary [100]-oriented PMN-32PT crystal, the [100]-oriented 6PSN-61PMN-33PT crystal exhibited excellent optical properties, including high transmittance, low refractive index, weak frequency dispersion, and low reflection and absorption coefficients. All these differences can be attributed to the structural changes of the 6PSN-61PMN-33PT crystal, such as its large lattice size and increased band gap. The crystal's transmittance was significantly improved after alternating current electric field poling due to the increased domain size and the order domain structure. The largest transmittance for the 6PSN-61PMN-33PT crystal was up to 66%. Our experimental results indicate that the ternary 6PSN-61PMN-33PT ferroelectric single crystal has great application potential in the optical field.

Keywords: PSN-PMN-PT ferroelectric crystals; optical properties; domain structure; band gap energy; AC-poled

Citation: Long, W.; Fan, X.; Fang, P.; Li, X.; Xi, Z. Optical Properties and Band Gap of Ternary PSN-PMN-PT Single Crystals. *Crystals* **2021**, *11*, 955. https://doi.org/10.3390/cryst11080955

Academic Editor: Paul R. Raithby

Received: 16 July 2021
Accepted: 13 August 2021
Published: 16 August 2021

1. Introduction

Multifunctional materials with acoustic, optical, electrical, and magnetic properties are considered the mainstream of the future development in the materials science field. Ferroelectric crystals integrated with excellent optical and electrical properties have great application prospect in advanced devices such as electro-optic switches, electro-optic modulators, and light valves.

$PbTiO_3$-based relaxor ferroelectric crystals such as (1-x)$Pb(Mg_{1/3}Nb_{2/3})O_3$–$xPbTiO_3$ (PMN–PT) with a composition near the morphotropic phase boundary (MPB) have attracted a great deal of attention due to their remarkable electrical properties (d_{33} ~ 2500 pC/N, k_{33} ~ 95%, S ~ 1.7%) [1–5], which can be used in medical ultrasound probes, submarine sonars, military sensors, etc. PMN-PT crystals were recently found to have excellent optical properties, such as high light transmittance (70%) using an alternating current electric field [2], high optical damage threshold (1 GW/cm^3) [6], remarkable linear electro-optic coefficient (γ = 112–175 pm/V) [7,8], and low half wave voltage (V = 230 V) [8], which indicate the potential application of these crystals in the optical and nonlinear optical fields. Unfortunately, the inferior thermal stability caused by their relatively low Curie temperatures (Tc ~ 130–150 °C) and low rhombohedral to tetragonal phase transition temperature ($T_{r\text{-}t}$ ~ 60–90 °C) limits their applications at high temperatures [9,10].

To overcome these shortcomings and improve the Tc and the Tr–t, $Pb(Sc_{1/2}Nb_{1/2})O_3$ (PSN) was introduced into the PMN-PT because its Tc that is much quite higher than that of PMN [11–16]. A relatively high phase transition temperature (Tc > 200 °C) has been reported in PSN-PMN-PT single crystals at the MPB, with good piezoelectric d_{33}

(1260~1550 pC/N) [16]. On the other hand, the introduction of Sc^{3+} into $LiNbO_3$ ferroelectric crystal has been reported to increase the crystal's optical damage-resistance properties [17]. Therefore, we speculate that ternary PSN-PMN-PT crystal will have higher optical damage-resistance properties than PMN-PT crystal, indicating its potential application prospect in the optical field. At present, most studies focus on these crystals' electrical properties [11–16]. No study has yet focused on the optical properties of the ternary PSN-PMN-PT crystal, which are detrimental to the design of optical devices and the development of multifunctional materials.

This study investigates the optical properties and the interband transitions of a [100]-oriented ternary 6PSN-61PMN-33PT crystal. The effects of the polarization method on the optical transmittance are analyzed by domain configuration. The differences of the optical properties between the [100]-oriented 6PSN-61PMN-33PT and the [100]-oriented PMN-32PT are compared. The band gaps are calculated based on the optical spectra. Sellmeier optical coefficients are determined by fitting the Wemple and DiDomenico (WDD) single oscillator equation.

2. Materials and Methods

High-quality, large-size ternary $6Pb(Sc_{1/2}Nb_{1/2})O_3$-$61Pb(Mg_{1/3}Nb_{2/3})O_3$-$33PbTiO_3$ (6PSN-61PMN-33PT) and binary $68Pb(Mg_{1/3}Nb_{2/3})O_3$-$32PbTiO_3$ (68PMN-32PT) crystals (Figure 1) were grown using the Bridgman technique. High-purity PbO (99.99%), MgO (99.99%), Nb_2O_5 (99.99%), Sc_2O_3 (99.99%), and TiO_2(99.99%) powders were used as the starting materials. $ScNbO_4$ (SN) and $MgNb_2O_6$ (MN) were first synthesized as precursors. Subsequently, SN, MN, TiO_2, and PbO were weighed as the stoichiometric ratio and mixed together. The powders were pressed into a Pt crucible with a Pt lid. The Pt crucible was then put into an Al_2O_3 crucible and placed in the Bridgman crystal growth equipment. After the crystal growth, the crystal was separated by stripping the Pt crucible.

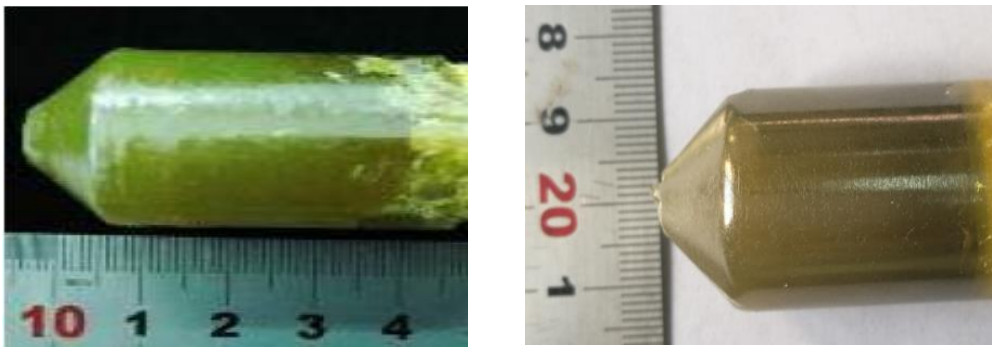

(**a**) (**b**)

Figure 1. Crystal grown using the Bridgman technique: nominal compositions of (**a**) 6PSN-61PMN-33PT and (**b**) PMN-32PT.

Laue diffraction was used to analyze the crystal orientation. Two crystals were cut into the slices of $5 \times 5 \times 0.8$ mm^3 perpendicular to the [100] direction. The crystalline structure was examined by X-ray diffraction (XRD, Bruker D2 focus). For the optical measurements, the 740 μm-thick specimens were polished using diamond-polishing compounds. The samples were then annealed to remove the residual stress derived from the polishing process (350 °C, 30 min).

The room-temperature optical transmission and absorption coefficient spectra of the [100]-oriented 6PSN-61PMN-33PT and PMN-32PT single crystals were measured in the wavelength range of 200–2500 nm through a UV–Vis–NIR spectrophotometer (Agilent, Cary 5000, NM, USA). The refraction parameters were tested using a spectroscopic ellipsometer (SE-VM, Eoptics, Wuhan, China) in the wavelength range of 380–1000 nm. The incident light angle was 65° during the measurement process. Silver paste was used to cover both sides of the (100) crystal face to load the external electric field on the single

crystals. The samples were dried at 70 °C for 20 min to ensure good electrical conductivity. The crystal samples were then poled at room-temperature for 15 min under a direct current electric field (20 kV/cm) and an alternating current electric field with a triangular waveform at 20 kV/cm and 5 Hz. The domain configurations were observed using a polarized light microscope (PLM, LEICADM2500P+7HMS, Leica, Germany) after the silver electrodes were removed using acetone.

3. Results and Discussions

The single crystal orientation has an effect on the optical properties due to various domain structures. Figure 2a,c shows the XRD pattern of the 6PSN-61PMN-33PT and 68PMN-32PT square slices. Only two diffraction peaks of (100) and (200) at 22° and 45° were obtained, indicating that the orientation of the two square slices was the [100] direction. We performed powder XRD to prove whether or not the two crystals were of perovskite structure (Figure 2b,d). As compared to $Pb(Mg_{1/3}Nb_{2/3})O_3$ (PDF#81-0861), standard perovskite structure peaks were obtained, indicating that the selected samples were of pure perovskite structure without any pyrochlore phase. Compared to those shown in Figure 2d, the diffraction peaks in Figure 2b slightly shifted towards a low angle, suggesting an increase of the lattice size in the 6PSN-61PMN-33PT crystals, which can be attributed to the large-ion Sc^{3+} (r_{ion} = 0.0745 nm) occupying the B-site to substitute the small-ion Mg^{2+} (r_{ion} = 0.072 nm) and Nb^{5+} (r_{ion} = 0.064 nm). Crystal lattice parameters (a = b = c = 4.0257 Å for 6PSN-61PMN-33PT, and a = b = c = 4.0226 Å for PMN-32PT) calculated by the software Jade further certify the increase of lattice size.

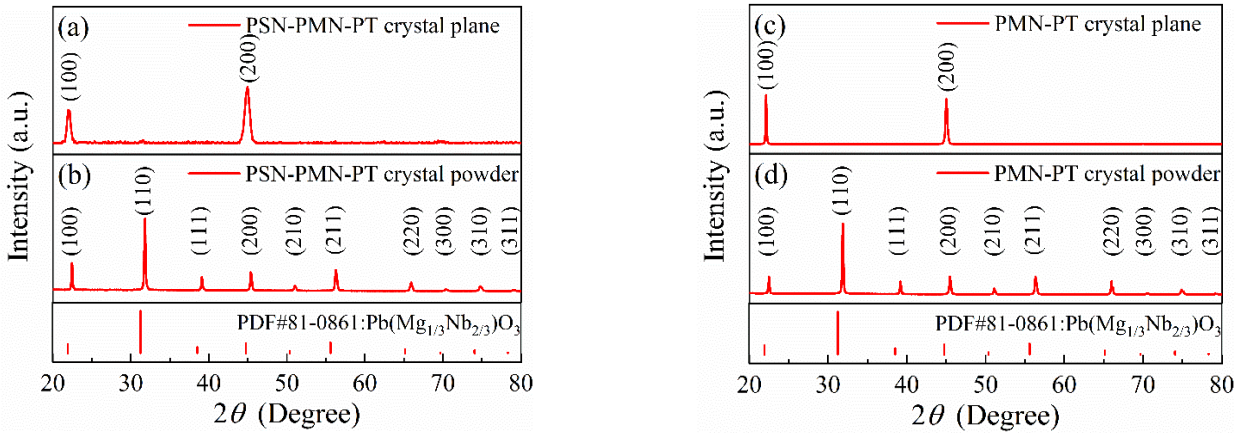

Figure 2. XRD diffraction patterns of crystals: (**a**) [100]-oriented 6PSN-61PMN-33PT; (**b**) powder X-ray diffraction patterns of 6PSN-61PMN-33PT and (**c**) [100]-oriented 68PMN-32PT; and (**d**) powder X-ray diffraction of 68PMN-32PT.

Excellent transmittance is a key factor in nonlinear optical materials. Figure 3 shows the transmittance spectra of the [100]-oriented 6PSN-61PMN-33PT and PMN-32PT crystals at different poled states, including the alternate current electric field-poled (AC-poled) state, direct current electric field-poled (DC-poled) state, and green state (unpoled) to explore the effects of the polarization process on the optical properties. All samples were transparent in the visible light and near-infrared regions in the wavelength range from 450 to 2500 nm. However, the transmittance rapidly decreased near 400 nm, showing an optical absorption edge in the ultraviolet region. The inset in Figure 3 shows the amplified plot of the transmittance spectra near the optical absorption edge. The wavelength of the absorption edge of the 6PSN-61PMN-33PT crystal was smaller than that of the binary PMN-32PT crystals, indicating a slight blue shift in the maximum absorption. The crystal transmittance after the AC poling sharply increased in the visible light region and obtained large values compared with the unpoled and DC-poled samples. In particular, for the [100]-oriented 6PSN-61PMN-33PT crystal, the highest transmittance of approximately 63% in the visible light range was obtained after the AC poling along the [100] direction. This value

was higher than that of the DC-poled (<50%) and unpoled (<37%) samples. These results provide an effective means of optimizing the optical performance of the ferroelectric crystal.

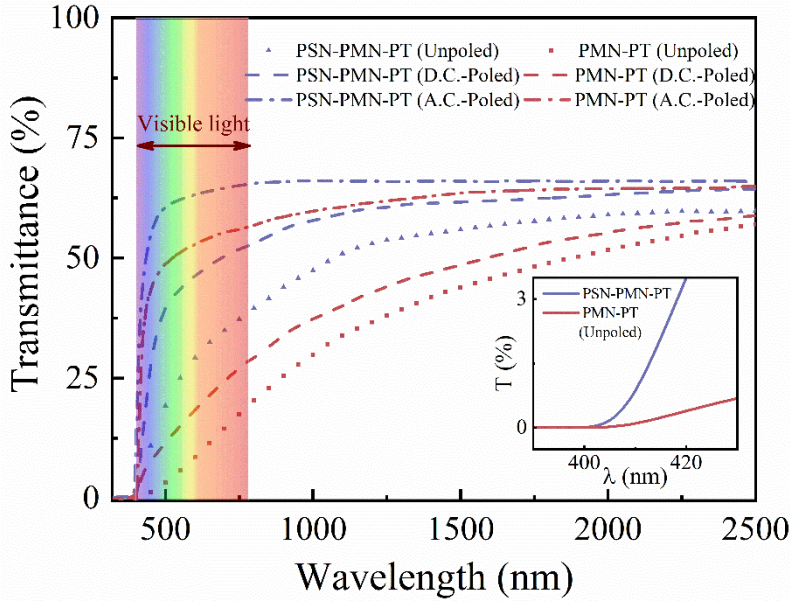

Figure 3. Transmittance spectra of the [100]-oriented 6PSN-61PMN-33PT and [100]-oriented PMN-32PT single crystals at different poled states (inset: enlarged version).

For ferroelectrics, the domain wall scattering is another main factor of the optical loss, except for the optical band gap [2,8]. Figure 4a–c shows the domain structure of the [100]-oriented 6PSN-61PMN-33PT crystal pretreated by different electric fields. For the unpoled sample (Figure 4a), most of the domains showed blurred margins and discontinuities, except for a few tiny domain bands, indicating a large domain wall density caused by the relatively small domain size. After the crystal was poled using the DC electric field, the domain size increased and the discontinuous domains showed an obvious decrease (Figure 4b). According to a previous report by Liu [18], this is a typical '4R' engineering domain configuration with 71° and 109° domain walls. For the AC-poled sample in Figure 4c, the domain configuration underwent amazing changes. The domain walls almost disappeared, suggesting the emergence of a monodomain state. Our experimental results are consistent with the theorical calculation results reported by Xu et al. [2,3,18,19]. Therefore, we propose that the decrease of domain walls density and ordered domain structure is beneficial to improve the crystal transmittance.

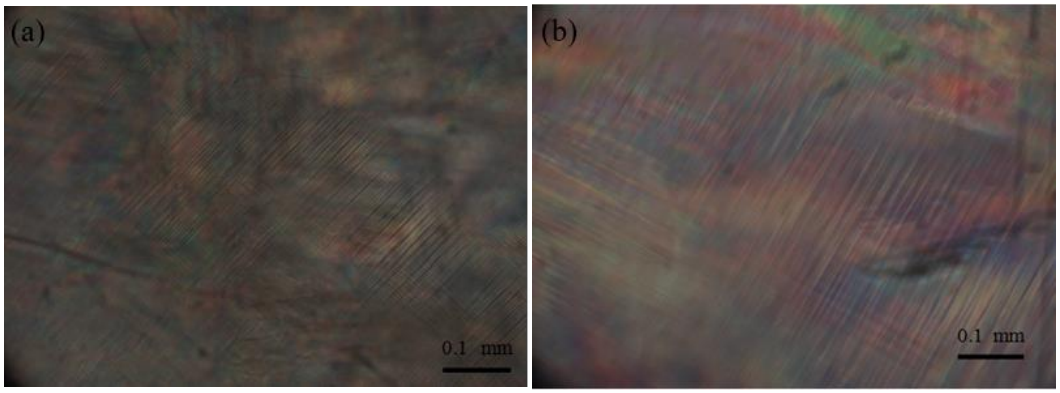

Figure 4. *Cont*.

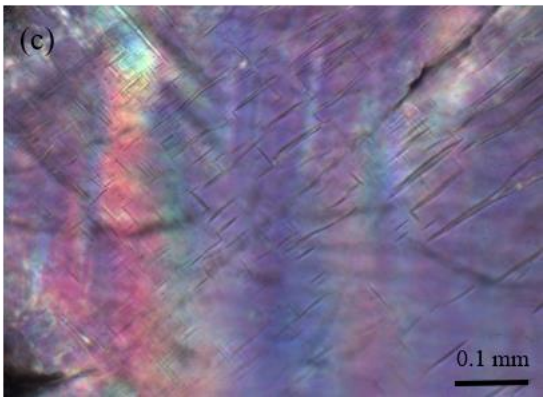

Figure 4. Domain morphology of the [100]-oriented 6PSN-61PMN-33PT (**a**) unpoled, (**b**) DC-poled, and (**c**) AC-poled crystals.

The refractive index is an important factor for material applications in the optical field. Figure 5 depicts the refractive indices of the [100]-oriented 6PSN-61PMN-33PT and PMN-32PT single crystals. Similar to those in most ABO_3-type perovskite compounds, the significant dispersion relationship and the rapid decrease of the refractive index with increasing wavelength from 375 nm to 1000 nm are presented in Figure 5a,b, indicating normal dispersion characteristics [20]. The ternary [100]-oriented 6PSN-61PMN-33PT crystal showed a smaller refractive index (n = 2.85–2.6) than PMN-32PT (n = 3.05–2.63) in the low wavelength range from 375 nm to 600 nm. This result indicates that the light with a wavelength between 375 nm and 600 nm had a higher propagation speed in the 6PSN-61PMN-33PT crystal than in the PMN-32PT crystal. Upon further increasing the wavelength above 600 nm, the refractive index values of both crystals gradually tended to become similar. In the same wavelength range, the change in the refractive index in the 6PSN-61PMN-33PT crystal was smaller than that in the PMN-32PT crystal. This shows the weaker dispersion in the 6PSN-61PMN-33PT crystal compared to that in the PMN-32PT crystal, which is conducive for improving the image quality.

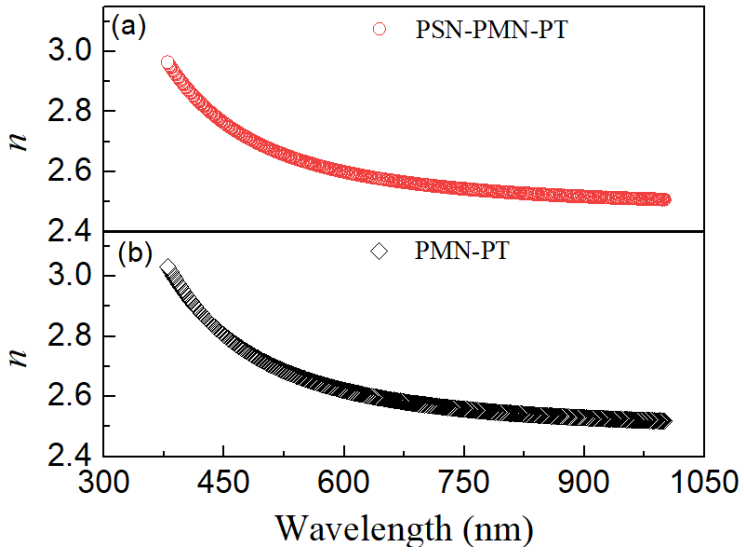

Figure 5. Wavelength dependence of the refractive index at room temperature for the (**a**) [100]-oriented 6PSN-61PMN-33PT and (**b**) [100]-oriented PMN-32PT single crystals.

For ferroelectrics with a perovskite structure, lattice dynamical theories indicate that the optical properties are mainly determined by the coupling of the d orbits in the B-site cation and the 2p orbits in the O anions related to each BO_6 octahedron [21], suggesting that the BO_6 octahedron plays a dominant role in the refractive index behavior in perovskite

structure ferroelectrics. Based on the results in Figure 2, we propose that the decrease of the refractive indices in the ternary 6PSN-61PMN-33PT crystals are related to the expansion of the BO_6 oxygen octahedron because the Sc^{3+} (r_{ion} = 0.0745 nm) ions enter into the B-site to replace the Mg^{2+} (r_{ion} = 0.072 nm) and Nb^{5+} (r_{ion} = 0.064 nm) ions [20,22].

Most ferroelectrics with oxygen octahedron as the basic structural unit are well known to have similar optical properties. Wemple and DiDomenico (WDD) introduced the single-oscillator dispersion model to study the relationship between the internal structure and the optical properties [23–25]:

$$n^2 - 1 = \frac{S_0 \lambda_0^2}{\left(1 - \lambda_0^2/\lambda^2\right)} = \frac{E_d E_0}{\left(E_0^2 - E^2\right)} \quad (1)$$

where n, λ_0, S_0, E_0, E_d, λ, and E are the refractive index, average oscillator position, average oscillator strength of the dipole oscillator, oscillator energy, dispersion energy, wavelength, and energy of the incident light, respectively. The oscillator energy E_0 is directly related to the energy band gap of the material. The dispersion energy E_d is closely related to the structural order of the material. The parameters in Equation (1) can be obtained by plotting $(n^2 - 1)^{-1}$ versus λ^{-2} and E^2, as shown in Figure 6. The perfect linear relationship in Figure 6 shows that it is reasonable to use the WDD dispersion model to study the 6PSN-61PMN-33PT and PMN-32PT ferroelectric crystals. Table 1 lists the calculated values of the Sellmeier optical coefficients for the 6PSN-61PMN-33PT and PMN-32PT crystals. E_0 and E_d of the PMN-32PT crystal were 5.6038 eV and 28.0141 eV, respectively. For the 6PSN-61PMN-33PT crystal, E_0 was 5.8288 eV, and E_d was 29.0784 eV, respectively. Our results are similar to those of the other PT-based materials with a ABO_3 perovskite structure [26–28].

The E_0 is considered the energy difference between the centers of gravity of the valence and conduction bands [29]. It is related to the direct bandgap E_{gd}, and a large bandgap E_{gd} corresponds to a large E_0. E_d is associated with the change in the chemical and structural order of a material, and a large order structure corresponds to a large E_d. Compared with the PMN-32PT, the 6PSN-61PMN-33PT crystal showed larger E_0 and E_d values (see Table 1). Therefore, we suggest that the 6PSN-61PMN-33PT crystal had a larger band gap and structure order than the PMN-32PT crystal [20,21].

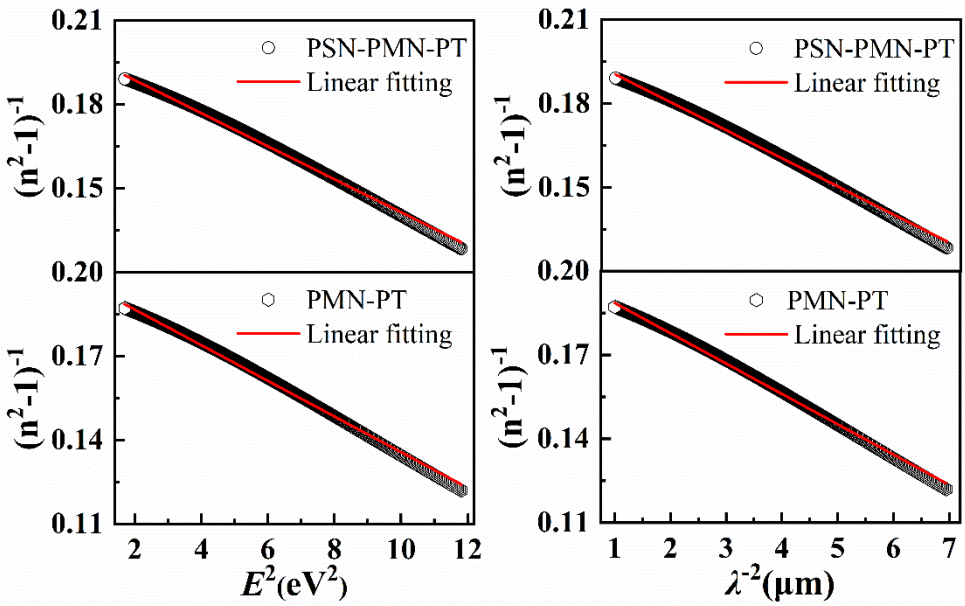

Figure 6. Dependence of $(n^2 - 1)^{-1}$ on E^2 and $(n^2 - 1)^{-1}$ on λ^{-2} for the 6PSN-61PMN-33PT and PMN-32PT single crystals.

Table 1. WDD optical parameters of the Pb-based ferroelectric single crystals at room temperature.

Composition	S_0 (10^{14} m^{-2})	λ_0 (μm)	E_0 (eV)	E_d (eV)	Ref.
6PSN-61PMN-33PT	0.9960	0.2238	5.8288	29.0784	This work
68PMN-32PT	0.9234	0.2330	5.6038	28.0141	This work
PZN–4.5%PT	0.8	0.227	5.46	22.52	[26]
24PIN-43PMN-33PT	1.047	0.206	6.032	29.34	[27]
Mn-15PIN-57PMN-28PT	1.178	0.215	6.06	28.73	[28]

Figure 7 shows the change in optical absorption coefficient α of the 6PSN-61PMN-33PT and PMN-32PT crystals as a function of the wavelength. A sharp absorption was observed near 500 nm, which can be interpreted by the mechanism of the band-to-band transition. Compared to that of the binary PMN-32PT crystal, the absorption wavelength of the ternary 6PSN-61PMN-33PT crystal was lower, indicating a larger optical band gap. In addition, the 6PSN-61PMN-33PT crystal showed a smaller light absorption (marked in ellipse) in the visible light region compared to the PMN-32PT crystal. The inset of Figure 7 shows the change in the reflection R as a function of the wavelength. R is calculated by Equation (2) under normal incidence,

$$R = \frac{(n-1)^2}{(n+1)^2} \tag{2}$$

where the n is the refractive index. The R of the PMN-32PT crystal was higher than that of the 6PSN-61PMN-33PT crystal with the wavelength increasing from 350 nm to 1000 nm. This result indicates a larger optical loss in the PMN-32PT crystal compared to the 6PSN-61PMN-33PT crystal.

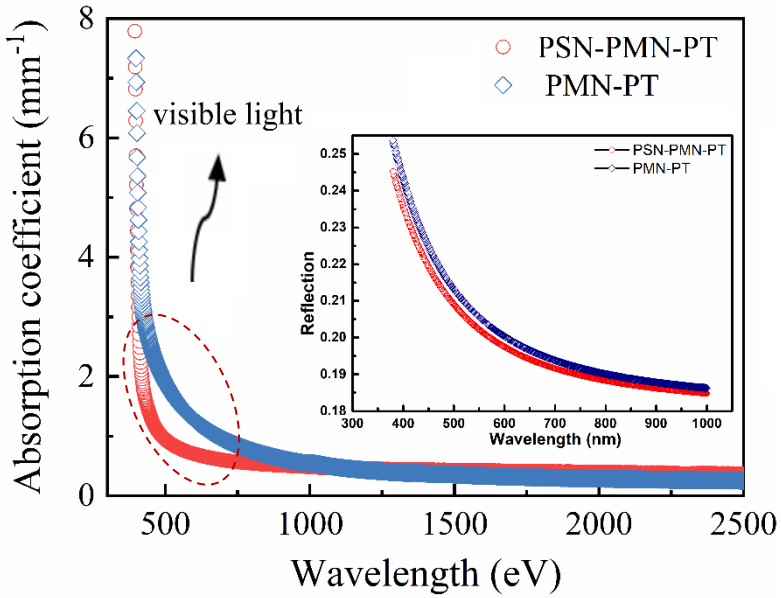

Figure 7. Optical absorption coefficient and reflectance (inset) of the 6PSN-61PMN-33PT and PMN-32PT crystals as a function of the wavelength.

Near the basic absorption edge, the absorption coefficient of the electron band-to-band transitions follows the following law [30]:

$$\alpha \propto (h\upsilon - E_g)^m \tag{3}$$

where $h\upsilon$ is the photon energy; E_g is the allowed optical energy gap; and m is the exponent characterizing the optical transition mechanism. In the allowed direct transition, $m = 1/2$, and the valence band transits vertically to the conduction band only under the action

of photons. In the indirect transition, $m = 2$, the electrons transit from the top of the valence band to the bottom of the conduction band with the participation of photons and suitable phonons.

The photon energy dependence of $(\alpha h\nu)^2$ and $(\alpha h\nu)^{1/2}$ for the [100]-oriented 6PSN-61PMN-33PT and PMN-32PT single crystals is shown in Figure 8a,b to investigate the absorption characteristics of the relaxor PT-based ferroelectric single crystal. The direct band gap energy (E_{gd}) of the samples was determined by extrapolating the linear portion of the curve to zero. The E_{gd} of the 6PSN-61PMN-33PT single crystal (i.e., 3.22 eV) was higher than that of the PMN–32PT single crystal (i.e., 3.18 eV), which is in agreement with the results shown in Figure 3. For the indirect band gap energy (E_{gi}), Equation (3) becomes

$$\alpha \propto (h\upsilon - E_{gi} \pm E_p)^2 \quad (4)$$

$$E_{g1} = E_{gi} + E_p \quad (5)$$

$$E_{g2} = E_{gi} - E_p \quad (6)$$

where E_{gi} is the indirect band gap energy, and E_p is the phonon energy. The E_{g1} and E_{g2} values were obtained by extrapolating $(\alpha h\nu)^{1/2}$ versus $h\nu$curves to zero (Figure 8b). Therefore, the indirect band gap energy $E_{gi} = 1/2(E_{g1} + E_{g2})$ and the phonon energy $E_p = 1/2(E_{g1} - E_{g2})$ could be obtained. Table 2 lists the direct band gap E_{gd} = 3.2228 eV, indirect band gap E_{gi} = 3.066 eV, and phonon energy E_p = 0.0697 eV for the 6PSN-61PMN-33PT single crystal; and E_{gd} = 3.1838 eV, E_{gi}= 2.952 eV, and E_p = 0.0913 eV for the PMN-32PT single crystal. The 6PSN-61PMN-33PT crystal evidently showed a larger direct bandgap energy and indirect bandgap energy compared to the PMN-32PT crystal, which may lead to differences in their optical properties. Our results are similar to the PZN-7PT and 24PIN-43PMN-33PT crystals in [27,31].

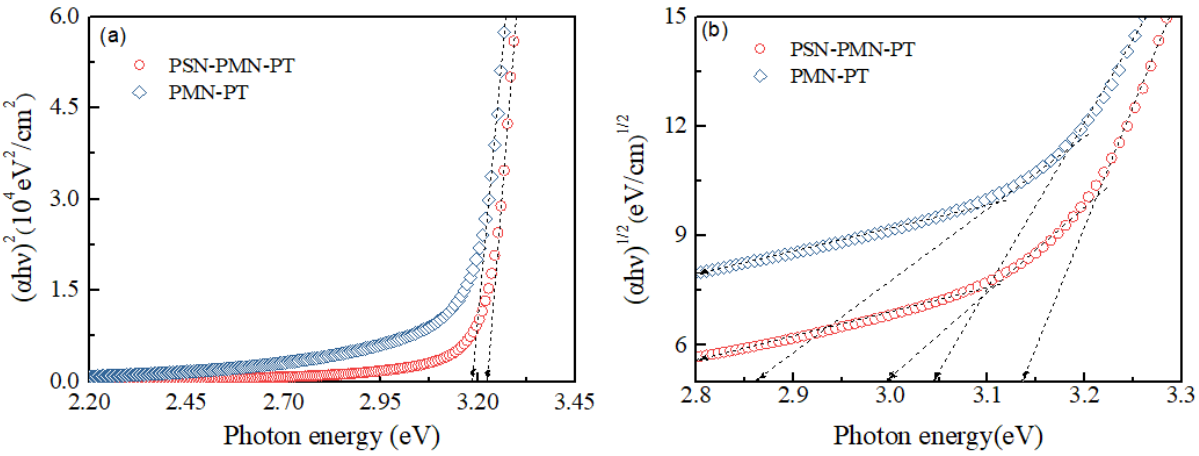

Figure 8. (**a**) $(\alpha h\nu)^2$ versus $h\nu$ of the 6PSN-61PMN-33PT and PMN-32PT single crystals. (**b**) $(\alpha h\nu)^{1/2}$ versus $h\nu$ of the 6PSN-61PMN-33PT and 68PMN-32PT single crystals.

Table 2. Values of the direct band gap E_{gd}, indirect band gap E_{gi}, and energy of the phonon E_p for the PT-based ferroelectric single crystals.

Composition	E_{gd} (eV)	E_{g1} (eV)	E_{g2} (eV)	E_{gi} (eV)	E_p (eV)	Ref.
PSN-PMN-PT	3.2228	3.1357	2.9963	3.0660	0.0697	This work
PMN-PT	3.1838	3.0438	2.8611	2.9524	0.0913	This work
PZN-7PT	3.144	3.012	2.817	2.915	0.097	[31]
24PIN-43PMN-33PT	3.115	–	–	–	–	[27]

4. Conclusions

This study systematically investigated the optical properties and band gap of [100]-oriented 6PSN-61PMN-33PT and PMN-32PT relaxor-based ferroelectric single crystals using the transmission spectra, refractive indices, WDD single-oscillator dispersion relation, and Tauc law. Consequently, the 6PSN-61PMN-33PT crystal showed superior optical properties, such as high transmittance, low refractive index, low reflection coefficient, and low light absorption compared to the 68PMN-32PT crystal. This outstanding performance makes the 6PSN-61PMN-33PT crystal a candidate optical material. The optical properties of a crystal can be controlled by the polarization process. The improvement in the transmittance through AC poling was more obvious than that in the DC polarization, which is related to the increased domain size and the order domain structure. The 6PSN-61PMN-33PT crystal showed an enlarged lattice size, a larger bandgap energy, and structure order compared to the PMN-32PT crystal, leading to differences in their optical properties.

Author Contributions: Methodology, W.L.; investigation, W.L., X.F.; resources, Z.X.; writing—original draft preparation, W.L., X.F.; writing—review and editing, X.L., P.F.; visualization, P.F.; supervision, X.L.; project administration, X.L.; funding acquisition, Z.X. All authors have read and agreed to the published version of the manuscript.

Funding: This work was financially supported by the National Natural Science Foundation of China (No. 51602242, 51772235, 11704249); the National Science Foundation of Shaanxi Province of China (No. 2019JM164); as well as the Key Laboratory Foundation of Shaanxi Province of China (No. 2020JS056).

Institutional Review Board Statement: Not applicable.

Informed Consent Statement: Not applicable.

Data Availability Statement: Contact the authors directly for the data of the presented graph or any other data used in this article.

Conflicts of Interest: There are no conflict to declare.

References

1. Chang, Y.F.; Wu, J.; Liu, Z.; Sun, E.W.; Liu, L.; Kou, Q.W.; Li, F.; Yang, B.; Cao, W. Grain-oriented ferroelectric ceramics with single-crystal-like piezoelectric properties and low texture temperature. *ACS Appl. Mater. Interface* **2020**, *12*, 38415–38424. [CrossRef]
2. Qiu, C.R.; Wang, B.; Zhang, N.; Zhang, S.J.; Liu, J.F.; Walker, D.; Wang, Y.; Tian, H.; Shrout, T.R.; Xu, Z.; et al. Transparent ferroelectric crystals with ultrahigh piezoelectricity. *Nature* **2020**, *577*, 350–354. [CrossRef]
3. Li, F.; Zhang, S.J.; Damjanovic, D.; Chen, L.Q.; Shrout, T.R. Local structural heterogeneity and electromechanical responses of ferroelectrics: Learning from relaxor ferroelectrics. *Adv. Funct. Mater.* **2018**, *28*, 1801504. [CrossRef]
4. Park, S.E.; Shrout, T.R. Ultrahigh strain and piezoelectric behavior in relaxor based ferroelectric single crystals. *J. Appl. Phys.* **1997**, *82*, 1804–1811. [CrossRef]
5. Li, F.; Cabral, M.J.; Xu, B.; Cheng, Z.X.; Dickey, E.C.; LeBeau, J.M.; Wang, J.L.; Luo, J.; Taylor, S.; Hackenberger, W.; et al. Giant piezoelectricity of Sm-doped $Pb(Mg_{1/3}Nb_{2/3})O_3$-$PbTiO_3$ single crystals. *Science* **2019**, *364*, 264–268.
6. Fang, Z.; Jiang, X.D.; Tian, X.; Zheng, F.J.; Cheng, M.Q.; Zhao, E.D.; Ye, W.N.; Qin, Y.L.; Zhang, Y.C. Ultratransparent PMN-PT electro-optic ceramics and its application in optical communication. *Adv. Opt. Mater.* **2021**, *9*, 2002139. [CrossRef]
7. Hu, Q.Y.; Yang, R.; Zhao, Y.; Zhao, W.G.; Liu, X.; Fu, X.T.; Luan, P.; Song, K.X.; Zhuang, Y.Y.; Xu, Z.; et al. Achieve single domain state in (111)-oriented rhombohedral phase PMN-PT relaxor ferroelectric single crystals for electro-optical application. *Appl. Phys. Lett.* **2019**, *115*, 222901. [CrossRef]
8. Kamzina, L.S.; Wei, R.; Li, G.; Zeng, J.; Ding, A. Electro-optical properties of PMN–xPT compounds: Single crystals and transparent ferroelectric ceramic. *Phys. Solid State* **2011**, *52*, 2142–2146. [CrossRef]
9. Li, X.J.; Liu, P.; Xi, Z.Z.; Long, W.; Fang, P.Y.; Zhao, X.G. Thermal expansion and phase transition in [1]-oriented $0.69Pb(Mg_{1/3}Nb_{2/3})O_3$–$0.31PbTiO_3$ single crystal. *J. Alloys Compd.* **2014**, *613*, 8–12. [CrossRef]
10. Sun, E.W.; Cao, W.W. Relaxor-based ferroelectric single crystals: Growth, domain engineering, characterization and applications. *Prog. Mater. Sci.* **2014**, *65*, 124–210. [CrossRef]
11. Wang, Z.J.; Li, X.Z.; He, C.; Liu, Y.; Han, S.J.; Pan, S.L.; Long, X.F. Characteristic electrical properties of $Pb(Sc_{1/2}Nb_{1/2})O_3$–$PbTiO_3$ ferroelectric crystals. *J. Mater. Sci.* **2015**, *50*, 3970–3975. [CrossRef]
12. Ursic, H.; Tellier, J.; Holc, J.; Drnovek, S.; Kosec, M. Structural and electrical properties of 0.57PSN–0.43PT ceramics prepared by mechanochemical synthesis and sintered at low temperature. *J. Eur. Ceram. Soc.* **2012**, *32*, 449–456. [CrossRef]

13. Li, X.J.; Jing, Q.; Xi, Z.Z.; Long, W.; Fang, P.Y. Large piezoelectric stability and low polarization fatigue in 6Pb($Sc_{1/2}Nb_{1/2}$)O_3-70Pb($Mg_{1/3}Nb_{2/3}$)O_3-24$PbTiO_3$ crystals. *J. Electron. Mater.* **2019**, *48*, 2168–2173. [CrossRef]
14. Li, X.J.; Fan, X.; Long, W.; Fang, P.Y.; Guo, F.F.; Xi, Z.Z. Laser-modulated reversible polarization and enhanced electrical properties in PSN-PMN-PT ferroelectric crystal. *J. Mater. Sci.* **2021**, *56*, 10477–10487. [CrossRef]
15. Gou, Y.P.; Xu, H.Q.; Lou, H.S.; Xu, G.S.; Yin, Z.W. Growth and electrical properties of Pb($Sc_{1/2}Nb_{1/2}$)O_3–Pb($Mg_{1/3}Nb_{2/3}$)O_3–$PbTiO_3$ ternary single crystals by a modified Bridgman technique. *J. Cryst. Growth* **2001**, *226*, 111–116.
16. Wang, Z.J.; He, C.; Qiao, H.M.; Pang, D.F.; Yang, X.M.; Zhao, S.G.; Li, X.Z.; Liu, Y.; Long, X.F. In situdi-piezo-ferroelectric properties and domain configurations of Pb($Sc_{1/2}Nb_{1/2}$)O_3-Pb($Mg_{1/3}Nb_{2/3}$)O_3-$PbTiO_3$ ferroelectric crystals. *Cryst. Growth Des.* **2018**, *18*, 145–151. [CrossRef]
17. Zhen, X.H.; Li, Q.; Li, H.T.; Xu, Y.H.; Zhao, L.C. Growth and optical damage resistance of Sc, Er, Co-doped $LiNbO_3$ crystals. *Cryst. Res. Technol.* **2005**, *40*, 649–653. [CrossRef]
18. Liu, J.F.; Qiu, C.R.; Qiao, L.; Song, K.X.; Guo, H.S.; Xu, Z.; Li, F. Impact of alternating current electric field poling on piezoelectric and dielectric properties of Pb(In1/2Nb1/2)O3–Pb(Mg1/3Nb2/3)O3–PbTiO3 ferroelectric crystals. *J. Appl. Phys.* **2020**, *128*, 094104. [CrossRef]
19. Qiu, C.R.; Xu, Z.; An, Z.Y.; Liu, J.F.; Zhang, G.J.; Zhang, S.J.; Chen, L.Q.; Zhang, N.; Li, F. In-situ domain structure characterization of Pb($Mg_{1/3}Nb_{2/3}$)O_3-$PbTiO_3$ crystals under alternating current electric field poling. *Acta Mater.* **2021**, *210*, 116853. [CrossRef]
20. Wu, Y.; Hu, Y.Q.; Xue, S.D.; Zhao, X.Y.; Wang, F.F.; Tang, Y.X.; Duan, Z.H.; Shi, W.Z.; Luo, H.S.; Sun, R.B. Optical dispersion and bandgap of pure and Mn-doped 0.92$Na_{0.5}Bi_{0.5}TiO_3$-0.08$K_{0.5}Bi_{0.5}TiO_3$ lead-free single crystals. *J. Am. Ceram. Soc.* **2019**, *103*, 1–7.
21. Hu, Y.Q.; Xie, Q.X.; Wu, Y.; Zhao, X.Y.; Tang, Y.X.; Wang, F.F.; Duan, Z.H.; Lin, D.; Luo, H.S.; Liang, R.H. Effect of Mn-doping on optical properties of lead-free ($K_{0.4}Na_{0.6}$)NbO_3 ferroelectric single crystals. *J. Eur. Ceram. Soc.* **2020**, *40*, 2917–2921. [CrossRef]
22. Yao, J.; Ge, W.; Yan, L.; Reynolds, W.; Li, J.; Viehland, D.; Kiselev, D.; Kholkin, A.; Zhang, Q.; Luo, H. The influence of Mn substitution on the local structure of $Na_{0.5}Bi_{0.5}TiO_3$ crystals: Increased ferroelectric ordering and coexisting octahedral tilts. *J. Appl. Phys* **2012**, *111*, 064109.
23. Wang, L.; Ren, W.; Ma, W.; Liu, M.; Shi, P.; Wu, X. Improved electrical properties for Mn-doped lead-free piezoelectric potassium sodium niobate ceramics. *AIP Adv.* **2015**, *5*, 097120. [CrossRef]
24. Drdomenico, M.; Wemple, S.H. Oxygen-octahedra ferroelectrics, I. theory of electro-optical and nonlinear optical effects. *J. Appl. Phys.* **1969**, *40*, 720–734. [CrossRef]
25. Brews, J.R. Energy band changes in perovskites due to lattice polarization. *Phys. Rev. Lett.* **1967**, *18*, 662–664. [CrossRef]
26. Bing, Y.H.; Guo, R.; Bhalla, A.S. Optical properties of relaxor ferroelectric crystal: Pb($Zn_{1/3}Nb_{2/3}$)O_3-4.5%$PbTiO_3$. *Ferroelectrics* **2000**, *242*, 1–11. [CrossRef]
27. Wu, F.M.; He, X.J.; Zhang, J.Y.; Yang, B.; Sun, E.W.; Jiang, J.X.; Cao, W.W. Optical bandgap and dispersions of 0.24Pb($In_{1/2}Nb_{1/2}$)O_3-0.43Pb($Mg_{1/3}Nb_{2/3}$)O_3-0.33$PbTiO_3$ single crystal poled along [11]c direction. *Opt. Mater.* **2016**, *60*, 101–104. [CrossRef]
28. Li, Y.; Tang, Y.X.; Wang, F.F.; Zhao, X.Y.; Chen, J.W.; Zeng, Z.; Yang, L.R.; Luo, H.S. Optical properties of Mn-doped 0.15Pb($In_{1/2}Nb_{1/2}$)O_3-0.57Pb($Mg_{1/3}Nb_{2/3}$)O_3-0.28$PbTiO_3$ single crystal. *Appl. Phys. A* **2018**, *124*, 276. [CrossRef]
29. Suchaneck, G.; Chernova, E.; Kleiner, A.; Liebschne, R.; Jastrabík, L.; Meyer, D.C.; Dejneka, A.; Gerlach, G. Vacuum-ultraviolet ellipsometry spectra and optical properties of Ba(Zr,Ti)O_3 films. *Thin Solid Films* **2017**, *621*, 58–62. [CrossRef]
30. Tacu, J.; Grigorovici, R.; Vanc, A. Optical Properties and Electronic Structure of Ge. *Phys. Stat. Sol.* **1966**, *15*, 627. [CrossRef]
31. Sun, E.W.; Zhang, R.; Wang, Z.; Xu, D.P.; Li, L.; Cao, W.W. Optical interband transitions in relaxor-based ferroelectric 0.93Pb($Zn_{1/3}Nb_{2/3}$)O_3-0.07$PbTiO_3$ single crystal. *J. Appl. Phys.* **2010**, *107*, 113532. [CrossRef]